

Host galaxy morphologies of X-ray selected AGN: assessing the significance of different black hole fueling mechanisms to the accretion density of the Universe at $z \sim 1$.

A. Georgakakis^{1*}, A. L. Coil², E. S. Laird³, R. L. Griffith⁴, K. Nandra³, J. M. Lotz⁵,
C. M. Pierce⁶, M. C. Cooper⁷, J. A. Newman⁸, A. M. Koekemoer⁹

¹National Observatory of Athens, V. Paulou & I. Metaxa, 11532, Greece

²Department of Physics and Center for Astrophysics and Space Sciences, University of California, San Diego, 9500 Gilman Dr., La Jolla, CA 92093

³Astrophysics Group, Blackett Laboratory, Imperial College, Prince Consort Rd, London SW7 2AZ, UK

⁴Jet Propulsion Laboratory, California Institute of Technology, Pasadena, CA 91109

⁵National Optical Astronomy Observatory, 950 North Cherry Avenue, Tucson, AZ 85719, USA

⁶Department of Physics, University of California, Santa Cruz, 1156 High Street, CA 95064, USA

⁷Steward Observatory, University of Arizona, 933 N. Cherry Ave., Tucson, AZ 85721-0065, USA

⁸University of Pittsburgh, Physics & Astronomy Department, 3941 O'Hara Street Pittsburgh, PA, 15260, USA

⁹Space Telescope Science Institute, 3700 San Martin Drive, Baltimore, MD 21218, USA

29 October 2018

ABSTRACT

We use morphological information of X-ray selected AGN hosts to set limits on the fraction of the accretion density of the Universe at $z \approx 1$ that is not likely to be associated with major mergers. Deep X-ray observations are combined with high resolution optical data from the Hubble Space Telescope in the AEGIS, GOODS North and GOODS South fields to explore the morphological breakdown of X-ray sources in the redshift interval $0.5 < z < 1.3$. The sample is split into disks, early-type bulge-dominated galaxies, peculiar systems and point-sources in which the nuclear source outshines the host galaxy. The X-ray luminosity function and luminosity density of AGN at $z \approx 1$ are then calculated as a function of morphological type. We find that disk-dominated hosts contribute 30 ± 9 per cent to the total AGN space density and 23 ± 6 per cent to the luminosity density at $z \approx 1$. We argue that AGN in disk galaxies are most likely fueled *not* by major merger events but by minor interactions or internal instabilities. We find evidence that these mechanisms may be more efficient in producing luminous AGN ($L_X > 10^{44} \text{ erg s}^{-1}$) compared to predictions for the stochastic fueling of massive black holes in disk galaxies.

Key words: Surveys – galaxies: starbursts – galaxies: evolution – X-rays: galaxies

1 INTRODUCTION

It is well established that Active Galactic Nuclei (AGN), which are signposts of accretion events onto the supermassive black holes (SMBHs) at the centres of galaxies, evolve strongly with cosmic time. Observational programs over the last 35 years have shown that the space density of these systems has a broad peak at $z \approx 1 - 3$ (e.g. Hasinger et al. 2005; Brusa et al. 2008; Silverman et al. 2008b; Aird et al. 2008) followed by a decline by almost 2 dex to the present day (e.g. Ueda et al. 2003; Hasinger et al. 2005; Barger et al. 2005). The physical interpretation of the observed rapid evolution of the AGN population however, is still a matter

of considerable debate. An important piece of the puzzle is the process that triggers the accretion of material onto the central SMBH.

A major galaxy merger is one of the popular mechanisms suggested to be responsible for fueling AGN. Numerical SPH (Smoothed Particle Hydrodynamic) simulations demonstrate that these violent events are very efficient in funneling gas to the nuclear galaxy regions (e.g. Hernquist 1989; Barnes & Hernquist 1991, 1996), where it can be consumed by the SMBH (Springel et al. 2005; Di Matteo et al. 2005). This scenario is also attractive because galaxy bulges are built parallel to the formation of SMBHs at their centres, thereby providing a physical interpretation for the observed tight correlation between bulge velocity dispersion and black hole mass in nearby galaxies (e.g. Ferrarese & Merritt 2000; Gebhardt et al. 2000). As a result, most semi-analytic cosmological simulations of galaxy formation (e.g. Somerville et al. 2008)

* email: age@astro.noa.gr

use major mergers as the primary mechanism for growing SMBHs. In this scenario, changes with redshift of the AGN space density are intimately related to the evolution of the major merger rate in the Universe.

Observations provide some support to the simulations described above, thereby suggesting that SMBHs can be fuelled by major mergers. In the local Universe for example, the population of Ultra-Luminous Infrared Galaxies (ULIRGs), which are dominated by major mergers (e.g. Surace et al. 1998; Borne et al. 2000; Farrah et al. 2001), include a large fraction of systems that show AGN signatures at optical and/or X-ray wavelengths (Sanders & Mirabel 1996; Franceschini et al. 2003). Additionally, a large fraction of luminous QSOs at low redshift are associated with either morphologically disturbed galaxies, suggesting ongoing tidal encounters (Canalizo & Stockton 2001; Guyon et al. 2006), or early type hosts with fine structure in their optical light distribution, indicative of past interactions (e.g. Canalizo et al. 2007; Bennert et al. 2008). Moreover, the excess of optical neighbours around $z < 0.4$ QSOs on small scales ($\approx 0.1 - 0.5$ Mpc) compared to L_* galaxies (Serber et al. 2006) and the higher fraction of QSO pairs with separations < 0.1 Mpc compared to the expectation on large (> 3 Mpc) scales (Hennawi et al. 2006; Myers et al. 2007), both suggest that galaxy mergers play an important role in the evolution of QSOs.

Despite the evidence above, it is also recognized that many AGN are not fueled by major mergers. In the nearby Universe for example, many Seyferts, which represent intermediate and low luminosity AGN, are associated with non-interacting spirals (e.g. Ho et al. 1997). The small scale environment (< 0.1 Mpc) of narrow line AGN, including a large fraction of Seyferts, in the Sloan Digital Sky Survey suggests that major galaxy interactions cannot explain the observed activity in the bulk of the population (Li et al. 2008). It is believed that the SMBHs of these systems accrete cold gas stochastically by mechanisms such as bar instabilities or minor tidal disruptions rather than major mergers (Hopkins & Hernquist 2006). It is also suggested that minor interactions and secular evolution are important at low redshift ($z \lesssim 1$) and low luminosities (e.g. $L_X \lesssim 10^{43} \text{ erg s}^{-1}$), while major mergers dominate at high redshifts and bright luminosities (e.g. Hasinger 2008; Hopkins & Hernquist 2006). Compared to models where major mergers drive the history of luminous accretion at all epochs (e.g. Hopkins et al. 2006; Somerville et al. 2008), the scenario above offers an alternative interpretation of the evolution of AGN based on a change with redshift of the dominant fueling mode of the SMBH.

Although there is no doubt that AGN are fueled by mechanisms that do not involve major mergers, as yet there are no robust limits on the relative contribution of such mechanisms to the total accretion luminosity. One way to address this issue is to study the morphology of the AGN host galaxies. In the standard view of major mergers any pre-existing disks are destroyed to form a bulge dominated remnant (Barnes & Hernquist 1996, e.g.). Therefore, AGN hosted by either disturbed/irregular systems or spheroidal galaxies are likely associated with ongoing or past major mergers, respectively. In contrast, AGN in disk galaxies are candidates for the stochastic SMBH fueling mode. Although recent simulations show that under certain conditions (e.g. high gas fraction) disks can survive major mergers (e.g. Springel & Hernquist 2005; Robertson et al. 2006; Hopkins et al. 2008; Governato et al. 2008), it is also claimed that the formation of a remnant with a large disk requires conditions which are often not associated with substantial SMBH fueling (e.g. Hopkins & Hernquist 2008a). The fraction of AGN in disk galaxy hosts therefore, remains a strong constraint on

Table 1. Chandra observations details

Survey	Obs. IDs	Exposure (Ms)	Area (deg ²)	All Sources (5)	0.5-7 keV Sources (6)
(1)	(2)	(3)	(4)	(5)	(6)
CDF-N	580, 957, 966, 967, 1671, 2232, 2233, 2234, 2344, 2386, 2421, 2423, 3293, 3294, 3388-3391, 3408, 3409	1.93	0.11	516	273
CDF-S	581 441 582 1672 2405 2239 2312 2313 2406 2409 1431 8591-8597 9575 9578 9593 9596 9718	1.93	0.06	428	245
AEGIS	3305, 4357, 4365, 5841-5854, 6210-6223, 6366, 6391, 7169 7180, 7181, 7187, 7188, 7236, 7237, 7238, 7239	0.19	0.63	1325	437

The columns are: (1): Survey name; (2): *Chandra* observation IDs used for each survey; (3) exposure time in Ms after cleaning for flares. In the case of the AEGIS survey with multiple pointings the median exposure time per pointing is listed; (4) total surveyed area in deg²; (5) total number of sources in each survey (6) number of 0.5-7 keV selected sources that overlap with the regions covered by the HST/ACS observations of each survey.

the fueling mechanism and/or the conditions under which SMBH growth occurs.

At low redshift for example, about 30 per cent of the powerful QSOs live in spirals (Canalizo & Stockton 2001; Guyon et al. 2006), while at $z \approx 1$, close to the peak of the accretion history of the Universe, about 20-30 per cent of the X-ray selected AGN are hosted by late-type disk galaxies (Pierce et al. 2007; Gabor et al. 2008). These observations are often interpreted as examples of SMBHs fueled by minor interactions and/or secular evolution. What is uncertain however, is the luminosity distribution of the AGN in disk hosts, i.e. what fraction of the AGN space and luminosity density is associated with this type of galaxy. This is essential to place a limit on the significance of minor interactions and/or internal instabilities to the accretion history of the Universe.

In this paper we address this issue by estimating, as a function of host galaxy morphology, the X-ray luminosity function and the X-ray luminosity density of X-ray selected AGN at $z \approx 1$. Our analysis provides a lower-limit to the fraction of AGN fuelled by secular evolution and minor mergers or equivalently an upper limit in the fraction of AGN in major mergers. For this exercise we use deep Chandra surveys with available multi-waveband Hubble Space Telescope (HST) observations. The fields of choice are the 2 Ms Chandra Deep Field North (CDF-North), the 2 Ms Chandra Deep Field South (CDF-South) and the All-wavelength Extended Groth strip International Survey (AEGIS; Davis et al. 2007). Using data from these programs has the advantage of publicly available follow-up observations, including deep ground-based optical photometry and extensive spectroscopy. Throughout this paper we adopt a cosmology with $H_0 = 70 \text{ km s}^{-1} \text{ Mpc}^{-1}$, $\Omega_M = 0.3$ and $\Omega_\Lambda = 0.7$.

2 DATA

2.1 X-ray observations

Table 1 presents information on the Chandra surveys of the AEGIS, CDF-North and CDF-South. The X-ray observations of the Extended Groth Strip consist of 8 ACIS-I (Advanced CCD Imaging Spectrometer) pointings, each with a total integration time of about 200 ks split in at least 3 shorter exposures obtained at different epochs. The CDF-North X-ray survey consists of 20 individual ACIS-I observations, which sum up to a total exposure time of 2 Ms. The Chandra data in the CDF-South have recently been sup-

plemented with new ACIS-I pointings, which have increased the total exposure time in that field to about 2 Ms.

The Chandra observations in the three fields above have been reduced and analysed in a homogeneous way using the methodology described by Laird et al. (2008). Briefly, the reduction used the CIAO data analysis software. After merging the individual observations into a single event file, we constructed images in four energy bands 0.5–7.0 keV (full), 0.5–2.0 keV (soft), 2.0–7.0 keV (hard) and 4.0–7.0 keV (ultra-hard). The count rates in the above energy intervals are converted to fluxes in the standard bands 0.5–10, 0.5–2, 2–10 and 5–10 keV, respectively. For the full, hard and ultra-hard bands this conversion involves an extrapolation from 7 to 10 keV. Sources in the flux range probed by the Chandra surveys listed in Table 1 have, on average, spectra similar to that of the cosmic X-ray Background in the 2–10 keV band, $\Gamma = 1.4$ (e.g. Hickox & Markevitch 2006). Therefore, to convert source count rates to fluxes we adopt a power-law X-ray spectrum with index $\Gamma = 1.4$ absorbed by the Galactic hydrogen column density appropriate for each field. Adopting $\Gamma = 1.9$ would decrease the estimated fluxes in the 0.5–10 keV band by about 30 per cent.

The source detection is a two pass process. A list of candidate sources is first constructed by running the WAVDETECT task of CIAO at a low detection threshold (10^{-4}). The total counts (source and background) at the position of each candidate source are then extracted within the 90 per cent Encircled Energy Fraction (EEF) radius of the Point Spread Function (PSF; see section 2.2. of Laird et al. 2009 for details). A local background value is determined by first excluding pixels within the 95 per cent EEF of each candidate WAVDETECT source and then summing up the counts in an annulus centered on the source with inner radius equal to 1.5 times the 90 per cent EEF radius and width of 50 arcsec. The probability that the candidate source is a random fluctuation of the background is estimated assuming Poisson statistics. The final catalogue is comprised of sources with Poisson probabilities $< 4 \times 10^{-6}$ in at least one of the energy bands defined above. We choose to work with sources selected in the 0.5–7 keV energy band because it provides higher sensitivity resulting in a larger sample size. As we will only use X-ray sources that overlap with the multi-waveband HST surveys (see below) of the AEGIS, CDF-North and CDF-South, in Table 1 we list the number of 0.5–7 keV selected sources that lie in the area covered by the HST observations.

The construction of the sensitivity maps is described by Georgakakis et al. (2008a). In this paper we will use the 1-D representation of the sensitivity map, the X-ray area curve, which provides an estimate of the total survey area in which a source with flux f_X can be detected. For simplicity we use area curves calculated in the standard way, i.e. by assigning a single limiting flux to a detection cell, instead of the Bayesian approach developed by Georgakakis et al. (2008a). The area curves for the HST subregions of the AEGIS, CDF-North and CDF-South are shown in Figure 1.

2.2 HST photometry

High resolution imaging observations from the Hubble Space Telescope (HST) are used to identify X-ray sources with optical counterparts and explore the morphology of their host galaxies.

The Advanced Camera for Surveys (ACS) aboard HST has been used to obtain deep images in the *V* (F606W, 2260s) and *I* (F814W, 2100s) filters over a $.1 \times 70.5$ arcmin² strip in the AEGIS field (Lotz et al. 2008b). The 5 sigma limiting magnitudes for a point source are $V_{F606W} = 28.14$ (AB) and $I_{F814W} = 27.52$

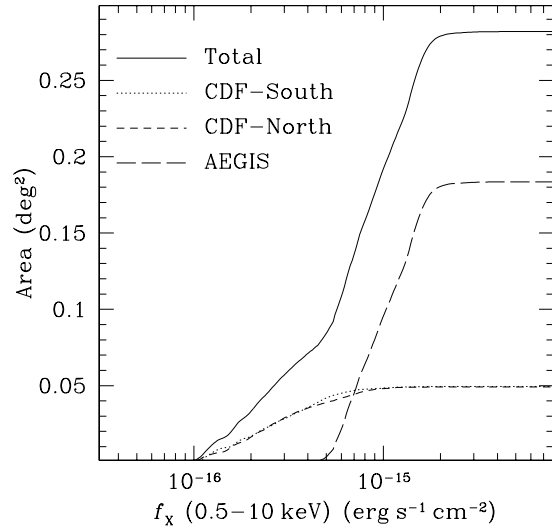


Figure 1. Sensitivity curves in the 0.5–10 keV band for the HST covered subregions of the CDF-South (dotted), CDF-North (short-dashed) and AEGIS (long-dashed). The continuous line is the sum of the individual curves.

(AB). For extended sources these limits are about 2 mag brighter. A total of 15 797 galaxies are detected to $I_{F814W} = 25$ mag.

The HST has also surveyed the central most sensitive part of the CDF-North and CDF-South with the ACS as part of the GOODS programme (Great Observatories Origins Deep Survey). These observations cover a combined area of about 0.08 deg² in four passbands, *B* (F435W), *V* (F606W), *i* (F775W) and *z* (F850LP). The survey setup, data reduction and source detection is described by Giavalisco et al. (2004). We use the version v1.0 of the mosaiced ACS images and the version v1.1 of the ACS multi-band source catalogs. The total exposure time of this data release is about 7200, 5000, 5000, and 10660 s in the *B*, *V*, *i* and *z* filters respectively. We use the *z*-band selected catalogues which include a total of 32048 and 29599 sources in the CDF-North and the CDF-South respectively.

The Likelihood Ratio method (LR; Sutherland & Saunders 1992; Ciliegi et al. 2003; Laird et al. 2008) is adopted to identify X-ray sources with optical counterparts. In this exercise we estimate the ratio between the probability that a source, at a given distance from the X-ray position and with a given optical magnitude, is the true counterpart and the probability that the source is a spurious alignment.

$$LR = \frac{q(m)f(r)}{n(m)}, \quad (1)$$

where $q(m)$ is the expected magnitude distribution of the true optical counterparts, $f(r)$ is the probability distribution function of the positional uncertainties in both the X-ray and the optical source catalogues and $n(m)$ is the background density of optical galaxies of magnitude m .

For the positional accuracy of the X-ray sources we adopt a Gaussian distribution with standard deviation estimated as a function of off-axis angle and total number of counts as described by Laird et al. (2008). The positional uncertainty of the HST source lists is also assumed to follow the normal distribution with FWHM (Full Width Half Maximum) of 0.07 arcsec for AEGIS (Lotz et al.

2008b) and 0.12 arcsec for the CDF-North and South. In equation 1, $f(r)$ is therefore assumed to be a Gaussian with standard deviation equal to the combined optical and X-ray source positional errors added in quadrature.

The a priori probability $q(m)$ that an X-ray source has a counterpart with magnitude m , is determined as follows. Firstly, the X-ray and optical source catalogues are matched by simply finding the closest counterpart within a fixed search radius of 2 arcsec. Secondly, a total of 100 mock catalogs are constructed by randomising the source positions of the HST catalog and the cross-matching is repeated. The magnitude distribution of the counterparts in the mock and the real catalogs are subtracted to determine the magnitude distribution of the true associations, $q(m)$.

Having estimated $f(r)$ and $q(m)$ we identify all possible counterparts to X-ray sources within a 4 arcsec radius and the LR of each one is estimated using equation 1. We consider as counterparts those galaxies with LR above a certain limit. The choice of the cutoff in LR is a trade off between maximum number of counterparts and minimum spurious identification rate. In order to assess how secure an optical counterpart is we use the reliability parameter defined by Sutherland & Saunders (1992)

$$\text{Rel}_i = \frac{\text{LR}_i}{\sum_j \text{LR}_j + (1 - Q)}, \quad (2)$$

where Rel_i is the reliability of the i optical counterpart of an X-ray source, the index j of the summation runs over all the possible counterparts within the search radius and Q is the fraction of X-ray sources with identifications to the magnitude limit of the optical survey. It can be shown that the sum of the reliabilities of individual counterparts equals the expected number of true associations (Sutherland & Saunders 1992). Comparison of $\sum_i \text{Rel}_i$ with the total number of counterparts with $\text{LR} > \text{LR}_{\text{limit}}$ provides an estimate of the spurious identification rate. By varying LR_{limit} one can minimise the number of false associations. We chose to use $\text{LR}_{\text{limit}} = 0.5$. At this cutoff, 78 (340/437), 74 (201/273) and 81 (199/245) per cent of the 0.5-7 keV selected X-ray sources in the AEGIS, CDF-North and CDF-South, respectively, have counterparts. These fractions are estimated using the total number of X-ray sources that overlap with the HST surveys of these fields. The estimated spurious identification rate is < 5 per cent.

2.3 Optical spectroscopy

Optical spectroscopy of X-ray sources in the AEGIS field is primarily from the DEEP2 redshift survey (Davis et al. 2003), which uses the DEIMOS spectrograph (Faber et al. 2003) on the 10 m Keck-II telescope to obtain redshifts for galaxies to $R_{AB} = 24.1$ mag. The observational setup uses a moderately high resolution grating ($R \approx 5000$), which provides a velocity precision of 30 km s^{-1} and a wavelength coverage of 6500–9100 Å. This spectral window allows the identification of the strong [O II] doublet 3727 Å emission line to $z < 1.4$. We use DEEP2 galaxies with redshift determinations secure at the $> 90\%$ confidence level (quality flag $Q \geq 3$; Davis et al. 2007). Spectroscopic observations targeting X-ray sources in AEGIS have also been carried out at the MMT using the Hectospec fiber spectrograph. Full details about these observations are given by Coil et al. (2009). A total of 449 X-ray sources were targeted with 5 Hectospec configurations. The data were taken in queue mode in May 2007, July 2007, and May 2008. Total integration times were 2 hours per configuration. The wavelength coverage is $\sim 4500 - 9000$ Å at 6 Å resolution. The data were re-

duced using the HSRED IDL reduction pipeline¹. Redshifts were measured either from emission lines from the AGN itself or HII regions if the host galaxy has ongoing star formation, or from the Ca H+K absorption features for lower luminosity AGN in early-type galaxies with little or no star formation. Although objects were targeted to $R_{AB} = 25$, the secure redshift identification rate was 50 per cent at $R_{AB} = 22.5$ mag and 15 per cent at $R_{AB} = 24.5$ mag. We obtained high-confidence redshifts for 230 sources, or 51% of the targeted sample. The resulting redshifts lie in the range $0 < z < 4$. The original Groth Strip has been targeted by a number of spectroscopic programs (Lilly et al. 1995; Brinchmann et al. 1998; Hopkins et al. 2000; Vogt et al. 2005) that have been compiled into a single database by Weiner et al. (2005)². The entire AEGIS overlaps with the Sloan Digital Sky Survey (SDSS) and therefore spectra for relatively bright galaxies and QSOs are also available (York et al. 2000). All the above diverse datasets provide high confidence spectroscopic redshifts for 159 0.5-7 keV selected X-ray sources in the HST/ACS subregion of the AEGIS.

Optical spectroscopy in the CDF-N and in the GOODS-North is available from either programmes that specifically target the X-ray population in these fields (e.g. Barger et al. 2003, 2005; Cowie et al. 2003) or the Keck Treasury Redshift Survey (TKRS; Wirth et al. 2004). The TKRS uses the DEIMOS spectrograph (Faber et al. 2003) at the Keck-II telescope to observe optically selected galaxies to $R_{AB} \approx 24.4$ mag in the GOODS-North. The publicly available catalogue consists of about 1400 secure redshifts. Out of the 201 X-ray sources selected in 0.5-7 keV band and optical counterparts with $\text{LH} > 0.5$, a total of 149 have spectroscopic redshifts.

There are many spectroscopic campaigns in the CDF-South. These include follow-up observations targeting specific populations, such as X-ray sources (Szokoly et al. 2004), K -band selected galaxies (Mignoli et al. 2005), and high redshift candidates (e.g. Dickinson et al. 2004; Stanway et al. 2004a,b), as well as generic spectroscopic surveys of faint galaxies in the GOODS area using the FORS2 (Vanzella et al. 2005, 2008) and VIMOS (Le Fèvre et al. 2004; Popesso et al. 2008) spectrographs at the VLT. There are 151 spectroscopic redshift estimates of the 199 0.5-7 keV selected X-ray sources with HST optical identifications.

2.4 Ground-based imaging and photometric redshifts

The spectroscopic observations are complemented by photometric redshifts calculated using ground-based imaging of the fields listed in Table 1. This provides a redshift (spectroscopic and photometric) completeness of 100 per cent for the magnitude limited sub-sample used in this paper (see next section for details on sample selection). We prefer the ground-based observations over the HST/ACS data for the photometric redshift estimation because they are deeper (AEGIS, CDF-North) and/or have more photometric bands, including imaging in the U filter.

The AEGIS is one of the fields of the deep synoptic Canada-France-Hawaii Telescope Legacy Survey (CFHTLS). These observations cover 1 deg^2 in the Extended Groth Strip in five filters ($ugriz$). We use the CFHTLS data from the T0003 release³, which reaches a limiting magnitude of $i_{AB} \approx 26.5$ mag. We use the photometric redshifts estimated by Ilbert et al. (2006) for sources

¹ See <http://www.astro.princeton.edu/~rcool/hsred>

² <http://saci.ucolick.org/verdi/public/index.html>

³ <http://terapix.iap.fr/article.php?idarticle=556>.

brighter than $i_{AB} \approx 25$ mag. The CFHTLS data overlap fully with area surveyed by the HST, thereby providing photometric redshifts for all HST sources with $i_{AB} \lesssim 25$ mag.

Deep multiwavelength imaging ($UBVRIz$) in the CDF-North has been presented by Capak et al. (2004). These observations cover about 0.2 deg^2 and extend beyond the CDF-North field of view. In this study we use the R -band selected sample comprising 47 451 sources to the limit $R_{AB} = 26.6$ mag (5σ). Photometric redshifts using these data have been presented by Georgakakis et al. (2007) using the methods described by Rowan-Robinson et al. (2005, 2008).

Ground-based photometric observations in 17 narrow and broad band filters have been obtained in an area of 1 deg^2 centered on the CDF-South as part of the COMBO-17 survey (Wolf et al. 2004). Although these observations are not as deep as the HST photometry the large number of filters provides excellent photometric redshift estimates to $R \approx 24$ mag (Wolf et al. 2004).

Figure 2 compares photometric with spectroscopic redshift estimates for X-ray sources in the CDF-South, CDF-North and AEGIS. Catastrophic redshifts, defined as those with $(z_{spec} - z_{phot})/(1 + z_{spec}) > 0.15$, represent 13, 16 and 32 per cent of the photometric redshift determinations of X-ray sources in the CDF-South, CDF-North and AEGIS, respectively. The accuracy of the photometric redshifts is estimated by the rms values of the quantity $(z_{spec} - z_{phot})/(1 + z_{spec})$ after excluding catastrophic redshifts. This is estimated 0.04, 0.06 and 0.05 for each of the surveys above, respectively. The CFHTLS photometric redshifts of X-ray sources suffer the largest catastrophic redshift rate. This is not surprising as these redshifts have been estimated using galaxy templates only (Ilbert et al. 2006) and also use a smaller number of photometric bands compared to the CDF-North and South photometric redshifts.

Uncertainties in the photometric redshifts are expected to have only a small impact on the results. As described in the next section, in the analysis we use a magnitude-limited sub-sample of X-ray sources ($I_{AB} < 23$ mag for the AEGIS and $z_{AB} < 24$ mag for the GOODS fields), for which the spectroscopic redshift completeness is about 88 per cent.

3 SAMPLE SELECTION AND MORPHOLOGICAL CLASSIFICATION

The sample consists of X-ray sources selected in the 0.5-7 keV band and in the redshift (photometric or spectroscopic) interval $z = 0.5 - 1.3$. The median redshift of the sample is ≈ 0.8 (see below), thereby allowing study of AGN hosts close to the peak of X-ray luminosity density of the Universe (e.g. Ueda et al. 2003).

Two main approaches are adopted in the literature for quantifying the optical morphology of galaxies. Visual inspection (e.g. Bell et al. 2005) and automated classification schemes, which measure morphology-sensitive structural parameters of the light distribution of galaxies. The latter methods include both non-parametric morphology estimators (Abraham et al. 1996; Lotz et al. 2004) and model fits to the optical profile of galaxies (e.g. Peng et al. 2002; Simard et al. 2002). These techniques have the advantage of objectivity and repeatability of the measurements. However, there are also limitations. In the case of AGN for example, the nuclear point source can be sufficiently bright to bias the estimation of structural parameters of the host galaxy light profile. The AGN light distribution (usually a point source) has to be modeled accurately and then subtracted from the image, before the morphology of the host

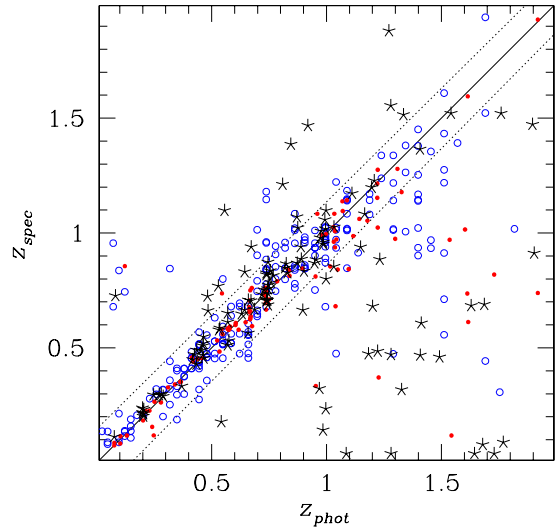


Figure 2. Photometric against spectroscopic redshift estimates for the X-ray sources in the CDF-South (red dots), CDF-North (open blue circles) and AEGIS (black stars). The continuous line is the $z_{phot} = z_{spec}$ relation, while the dashed lines correspond to $\delta z = \pm 0.2$. All sources with spectroscopic redshifts are plotted without applying any magnitude limit.

galaxy is determined. Although there has been progress recently in this direction (e.g. Kuhlbrodt et al. 2004; Simmons & Urry 2008; Gabor et al. 2008), the decomposition of the nuclear point source from the host galaxy is not straightforward, especially in the case of real galaxies with complex profiles, including disks, bulges, star-forming regions, dust lanes, etc. Additionally, non-parametric morphology estimators typically produce broad morphological classes. Irregular/interacting systems for example, maybe be hard to discriminate from late-type disk galaxies with bright star-forming regions superimposed on their spiral arms. It is also unclear how methods that fit models (e.g. Sersic function) to the galaxy light profile treat irregular or interacting galaxies and whether they can isolate such systems.

Eye-balling has issues of its own (e.g. Lotz et al. 2008a), but is best suited to this study which requires discrimination between spirals, bulges and irregular/interacting systems. Also, the presence of a photometrically important bulge or nuclear point source may bias automated morphological classification schemes against disks, even if they are large and obvious to the eye. We therefore choose to proceed with visual inspection of the HST images of X-ray AGN to classify them into 4 groups, disks (i.e. spirals), early-types (i.e. bulge dominated), peculiar/interacting and point sources. The latter class includes systems where the central AGN outshines the host galaxy and therefore morphological classification is not possible. This type of sources pose a challenge for any method that attempts to determine the light distribution of the underlying AGN host galaxy. The morphological classes have been determined independently by three classifiers (AG, ESL, ALC). In the analysis that follows we apply equal weights to each of the three independent classifications. We caution that faint or red disk-dominated sources may be misclassified as early-type hosts, thereby introducing a systematic bias against disks in our visual morphological classification. However, comparison with the classifications based on the Sersic index suggests that this bias is not affecting the results and conclusions (see section 5).

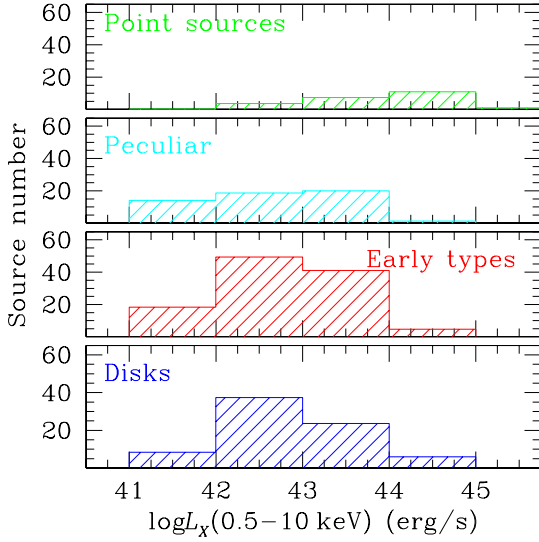


Figure 4. The X-ray luminosity distribution of X-ray selected AGN in the redshift interval $0.5 < z < 1.3$ as a function of host galaxy morphology.

We have empirically determined that reliable morphological classes are possible to $I_{AB} = 23$ mag for the AEGIS and $z_{AB} = 24$ mag for the deeper GOODS HST observations. Therefore, in the analysis that follows we use a magnitude-limited subsample of 454 (CDF-N: 156; CDF-S: 130; AEGIS: 168) X-ray sources brighter than $I_{AB} = 23$ and $z_{AB} = 24$ mag for the AEGIS and the GOODS fields respectively. This choice of magnitude limits has the additional advantage of high spectroscopic redshift completeness, thereby minimising the use of photometric redshifts. Secure spectroscopic redshifts are available for 398 of the 454 sources, of which 7 are Galactic stars. We use photometric redshifts for 56 sources only (CDF-N: 14; CDF-S: 13; AEGIS: 29) and therefore uncertainties in the estimation of photometric redshifts have a small impact on the results. If we further constrain the sample to the redshift interval $z = 0.5 - 1.3$ the total number of X-ray sources is 266 (median redshift 0.8). About 30 per cent of the sources in that sample have been assigned different morphological classifications by the three independent classifiers. We have tested that these differences do not affect the results and conclusions of the paper. In the next section for example, the X-ray luminosity function for different host galaxy morphological types is estimated. It is found that the X-ray luminosity functions for the 3 independent morphological classifications agree within the 1σ Poisson uncertainty. Examples of the HST images of X-ray sources classified as spirals, bulges and peculiars/interacting are shown in Figure 3.

4 LUMINOSITY FUNCTION

The binned X-ray luminosity function is derived using the standard non-parametric $1/V_{\max}$ method (Schmidt 1968). In this calculation we take into account the X-ray selection function, parameterised by the X-ray area curve, and the optical magnitude limit for morphological classification. The luminosity function, ϕ , in logarithmic luminosity bins, $d \log L$, is estimated from the relation

$$\phi d \log L = \sum_i \frac{1}{V_{\max,i}(L_X, M, z)}, \quad (3)$$

where $V_{\max,i}(L_X, M, z)$ is the maximum comoving volume for which the source i with X-ray luminosity L_X , absolute optical magnitude M and redshift z , satisfies the sample selection criteria, i.e. redshift range, apparent optical magnitude cutoff for morphological classification and X-ray flux limit. The maximum comoving volume is estimated from the relation

$$V_{\max,i}(L_X, M, z) = \frac{c}{H_0} \int_{z_1}^{z_2} \Omega(L_X, z) \frac{dV}{dz} dz dL, \quad (4)$$

where dV/dz is the volume element per redshift interval dz . The integration limits are $z_1 = z_L$ and $z_2 = \min(z_{\text{optical}}, z_U)$, where we have defined z_L, z_U the lower and upper redshift limits of the sample and z_{optical} is the redshift at which the source will become fainter than the optical magnitude cutoff for morphological classification. $\Omega(L_X, z)$ is the solid angle of the X-ray survey available to a source with luminosity L_X at a redshift z (corresponding to a flux f_X in the X-ray area curve). The uncertainty of a given luminosity bin is

$$\delta\phi^2 = \sum_i \left(\frac{1}{V_{\max,i}(L_X, M, z)} \right)^2. \quad (5)$$

In addition to the Poisson uncertainties above, differences among the morphological classes determined by the three independent classifiers are also accounted for in the error budget. We perform 1000 experiments in which the XLF is determined by randomly choosing for each source one of the three morphological types. This calculation provides for each luminosity bin an estimate of the 1σ rms of the XLF because of uncertainties in the morphological classifications. This is then added quadratically to the Poisson errors above. We note however, that Poisson errors typically dominate the uncertainties.

In order to convert absolute to apparent optical magnitude for the $1/V_{\max}$ calculation, optical k-corrections for both galaxy and QSO templates are used depending on the source morphological classification. For the early, disk and peculiar classes we adopt respectively the E/S0, Scd and Im galaxy type templates of Coleman et al. (1980), while for point sources we use the SDSS composite QSO spectrum of Vanden Berk et al. (2001). For AEGIS sources the optical k-corrections are estimated for the F814W filter, while for CDF-North and South X-ray AGN the F850LP filter is used in the calculations.

The X-ray luminosities in the 0.5–10 keV band are corrected for obscuration. The hardness ratio, HR, estimated in the 0.5–2 and 2–7 keV bands, is used to determine the column density, N_H , of individual sources assuming an intrinsic power-law X-ray spectrum with index $\Gamma = 1.9$ (e.g. Nandra & Pounds 1994). These column densities are then used to correct the observed L_X for absorption. We caution that for unobscured sources the assumption of $\Gamma = 1.4$ in section 2 overestimates the fluxes and hence the luminosities by about 30 per cent or $\Delta \log L_X = 0.1$. This effect therefore has only a minor impact on the estimated $L_X(0.5 - 10 \text{ keV})$. Additionally, unobscured sources ($N_H < 10^{22} \text{ cm}^{-2}$) are only a small fraction of the X-ray population at the depths of the CDF-North/South ($\approx 20\%$; Akylas et al. 2006) and the AEGIS ($\approx 40\%$; Georgakakis et al. 2006). When estimating the X-ray k-correction of individual sources for the $1/V_{\max}$ calculation we also take into account the intrinsic source N_H by adopting an absorbed power-law spectral energy distribution with $\Gamma = 1.9$ and photoelectric absorption cross sections as described by Morrison & McCammon (1983) for solar metallicity.

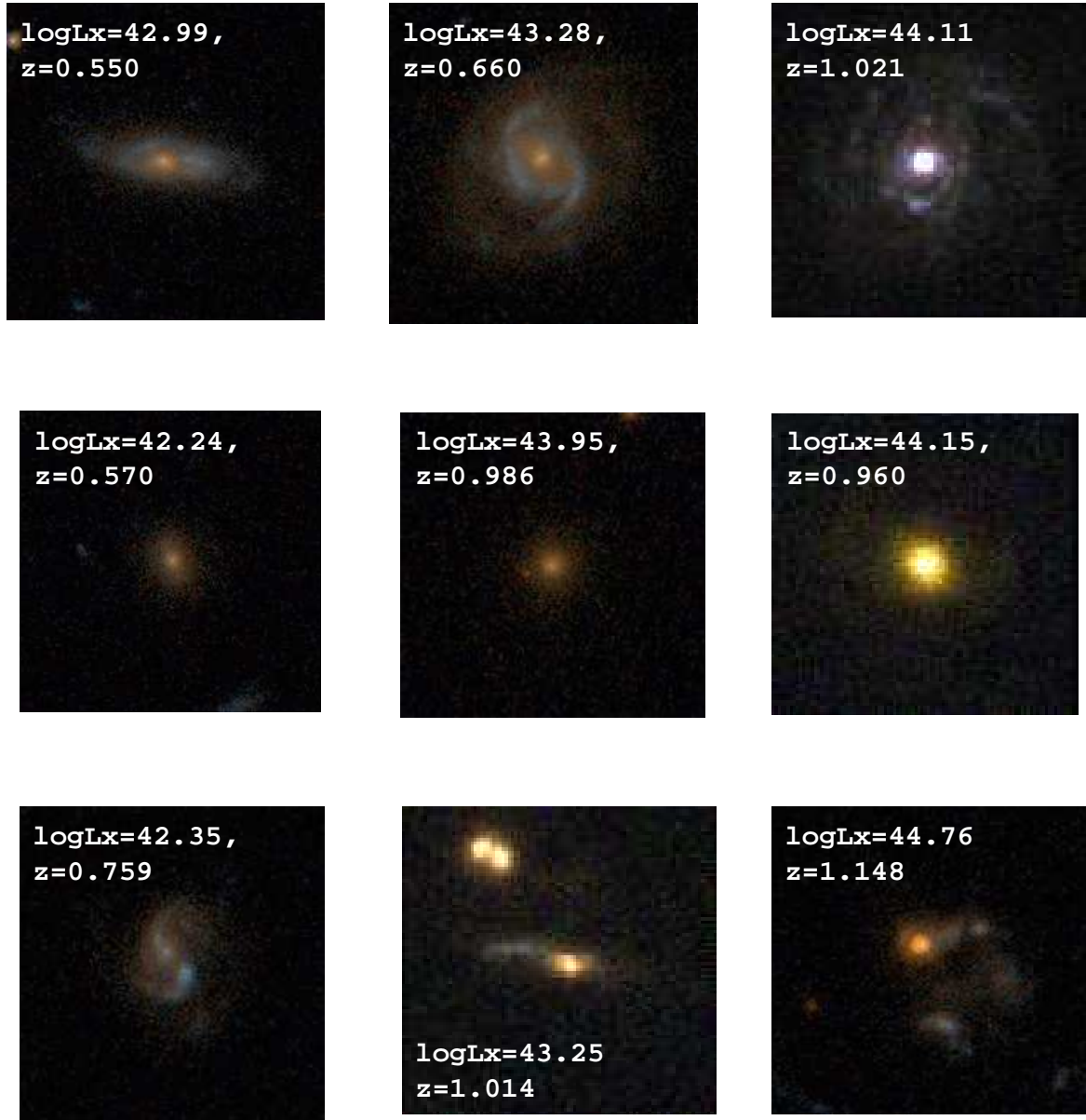


Figure 3. Examples of the HST true colour images of AGN classified as disks (top row), early-type (middle) and peculiar/interacting (bottom). The X-ray luminosity (0.5-10 keV) and redshift of each source are also shown. The images are about 5×5 arcsec in size.

5 RESULTS

Figure 4 plots the X-ray luminosity distribution of different AGN host galaxy morphological types. In agreement with previous studies, early-type bulge-dominated galaxies are the largest group, contributing 42 ± 4 per cent of the overall AGN population. These systems are either major merger remnants observed after the peak of the activity (e.g. Hopkins et al. 2006) or galaxies that have recently accreted cold gas, through minor interactions, which has resulted in the re-activation of the SMBH at their centres (e.g. Khalatyan et al. 2008). Alternative models for the fuelling of the SMBH in early type galaxies include recycled gas from dying stars (e.g. Ciotti & Ostriker 2007) or accretion from a cooling hot halo (e.g. Croton et al. 2006; Cattaneo & Teyssier 2007). Georgakakis et al. (2008b) have shown that the Asymmetry parameter (Abraham et al. 1996) distribution of X-ray AGN is broader

compared to optically selected early-type galaxies, suggesting low level morphological disturbances. This finding favors the scenario where AGN in early type hosts are associated with past merger events (minor or major).

Isolated disk galaxies represent about 28 ± 3 per cent of all AGN in Figure 4. These are systems in which the accretion onto the SMBH is likely to be triggered either by secular processes or minor tidal disruptions. Peculiars are about 20 ± 3 per cent of the AGN in our sample. These systems include ongoing major merger events. Their fraction may indicate the time-scale that major mergers can be identified morphologically (e.g. $\lesssim 10^9$ yrs; Lotz et al. 2008a). We caution however, that this fraction provides only an upper limit to this time-scale as the group of peculiars may also include Irregular galaxies that are not necessarily the product of major mergers. Finally, point-like sources in which the light from the central engine

outshines the host galaxy and does not allow morphological classification are a minority in our sample, 8 ± 2 per cent. As expected these sources are more numerous at bright X-ray luminosities. We note that the errors in the fractions above include uncertainties in the morphological classification of individual sources (see previous section) in addition to the Poisson errors.

The XLF, split into different host galaxy morphological types is plotted in Figure 5 and is presented in Table 2. The XLF of all AGN in the sample is in good agreement with the recent determination of Barger et al. (2005). Figure 6 and Table 3 present the fractional contribution of different morphological types to the total XLF. Early-type hosts are a major component of the XLF over almost the entire luminosity range, while point sources become dominant at $L_X(0.5 - 10 \text{ keV}) > 10^{44} \text{ erg s}^{-1}$. Disk hosts represent between 25-30% of the total XLF. The fraction of Peculiar hosts to the total XLF shows a weak decreasing trend with increasing luminosity, which is, however, within the uncertainties of the data.

The contribution of different morphological types to the luminosity density, $\phi \times L_X$, at $z \approx 1$ is shown in Figures 7 and 8. The results are also presented in Tables 2 and 3. Early-type hosts dominate the luminosity density up to $L_X(0.5 - 10 \text{ keV}) = 10^{44} \text{ erg s}^{-1}$. Above this limit point-like sources, i.e. QSOs, become the dominant component of $\phi \times L_X$. Disk and peculiar host galaxies represent about 11-35 per cent of the total AGN luminosity density.

We have checked how sensitive the results above are to the adopted method for determining the morphology of the AGN host galaxies. The classifications based on visual inspection are compared with those determined by fitting a single Sersic function to the AGN host galaxy light distribution (Griffith et al. in prep) using the Galfit code (Peng et al. 2002). A cutoff in the Sersic index, $n = 2.5$, is applied to discriminate between disk ($n < 2.5$) and bulge ($n > 2.5$) dominated galaxies. The Sersic model fits are reliable for systems where the central AGN does not dominate over the host galaxy light. This requirement translates to an empirically determined (visual inspection of the HST images) X-ray luminosity cut of $L_X(0.5 - 10 \text{ keV}) \approx 10^{44} \text{ erg s}^{-1}$. The comparison between the visual and Sersic index classifications is therefore restricted to sources with $L_X(0.5 - 10 \text{ keV}) < 10^{44} \text{ erg s}^{-1}$. We only consider sources that are visually classified “early” or “disk”. The class of “peculiar” is excluded because they comprise a large fraction of disturbed interacting/merging systems with complex optical light distributions. “Point” sources are also excluded to avoid uncertainties in the Sersic function fits associated with the presence of bright emission from the nuclear galaxy regions. The Sersic indices of both “peculiar” and “point sources” are hard to interpret in the context of disk or bulge dominated light profiles. It is found that although there is a discrepancy between the two classification methods (eyeballing vs Sersic index) for about 30% of the bulge and disk-dominated sources in the sample, the main results, e.g. the XLF of disks and bulges, are consistent within the 1σ errors and do not depend on the adopted method for determining the morphology of AGN hosts.

6 DISCUSSION

This paper estimates the space and luminosity density of X-ray selected AGN as a function of their host galaxy morphologies in an attempt to place constraints on the importance of major mergers, minor interactions and secular evolution to the accretion density of the Universe at $z \approx 1$. In the standard view of major gaseous mergers the disks of the participating galaxies are destroyed to form an

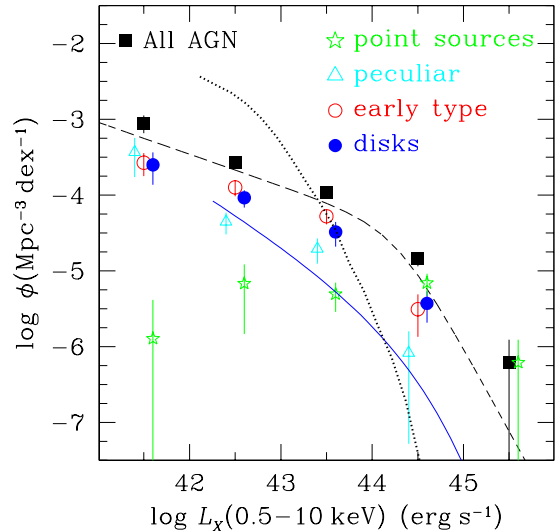


Figure 5. The 0.5-10 keV X-ray luminosity function for different host galaxy types. Stars (green) correspond to point sources, open triangles (cyan) are peculiar systems, open circles (red) are for early-type hosts and filled circles (blue) correspond to disk galaxies. For clarity triangles are offset horizontally by -0.1 dex in $\log L_X$, while stars and filled circles are offset by $+0.1$ dex. The filled squares (black) represent the total X-ray luminosity function, independent of host galaxy type. This is compared with the dashed line, which is the Barger et al. (2005) XLF at $z = 0.8$ (the median redshift of the sample) estimated in the 2-8 keV band and converted to the 0.5-10 keV band assuming a power-law X-ray spectrum with photon index $\Gamma = 1.9$. The dotted curve is the “maximal evolution” XLF prediction of the stochastic accretion mode of Hopkins & Hernquist (2006) at $z = 1$. This curve is adapted from Figure 6 of Hopkins & Hernquist (2006) adopting the Marconi et al. (2004) bolometric corrections. The continuous (blue) line is the updated version of the XLF for the stochastic accretion mode (P. F. Hopkins priv. communication) estimated using a revised AGN lightcurve, which results in more rapid evolution of the AGN emission after the peak of the accretion (see text for more details).

elliptical remnant. In this picture, disk hosts therefore indicate AGN fueled by minor interactions or internal instabilities.

It is found that disk galaxies represent about 25-34 per cent of the X-ray AGN number density and 19-35 per cent of the luminosity density of these systems (i.e. accretion density). These fractions are also almost independent of X-ray luminosity up to $L_X(0.5 - 10) \approx 10^{45} \text{ erg s}^{-1}$. Recently, Hopkins & Hernquist (2006) have developed a model for the stochastic fueling of SMBHs via e.g. bar instabilities or minor interactions. In their model this accretion mode produces relatively low luminosity AGN, while the bulk of the more luminous active SMBH are the result of major mergers. Figure 5 compares our results with the maximal X-ray luminosity function of the Hopkins & Hernquist (2006) stochastic accretion mode (dotted line). This model predicts a large number of low luminosity AGN, which can potentially explain the entire XLF below $\approx 10^{43} \text{ erg s}^{-1}$. Also plotted in Figure 5 is an updated version of the XLF for the stochastic accretion mode (P. F. Hopkins priv. communication; continuous line) in which the AGN lightcurve decays more rapidly than what is assumed by Hopkins & Hernquist (2006), in agreement with recent simulations (e.g. Younger et al. 2008) and observations of the Eddington ratio distribution of low redshift AGN in the SDSS (e.g. Hopkins & Hernquist 2008b). More quantitatively, in the work by Hopkins & Hernquist (2006)

Table 2. AGN XLF and luminosity density as a function of morphological type

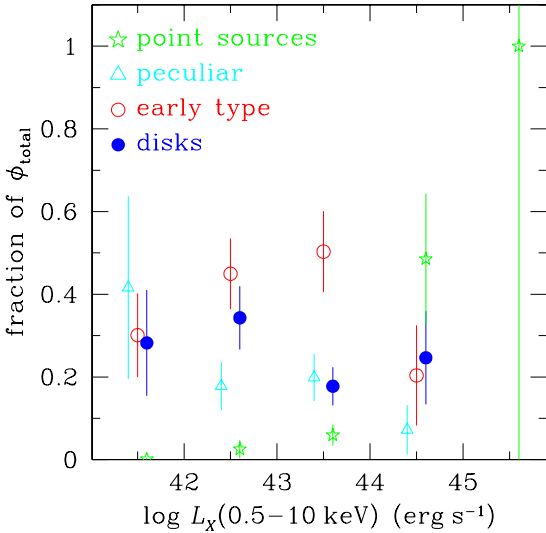
$\log L_X$ (erg s^{-1})	$\log \phi(L_X)$ ($\times 10^{-6} \text{ Mpc}^{-3}$)				$\log(L_X \phi(L_X))$ ($\times 10^{37} \text{ erg s}^{-1} \text{ Mpc}^{-3}$)			
	disk	early	peculiar	point	disk	early	peculiar	point
41–42	-3.60 ± 0.19	-3.57 ± 0.14	-3.43 ± 0.23	-5.89 ± 0.97	1.08 ± 0.19	1.17 ± 0.13	1.12 ± 0.16	-0.91 ± 0.97
42–43	-4.03 ± 0.11	-3.89 ± 0.10	-4.35 ± 0.13	-5.16 ± 0.34	1.49 ± 0.13	1.62 ± 0.13	1.01 ± 0.2	0.42 ± 0.25
43–44	-4.48 ± 0.15	-4.27 ± 0.09	-4.70 ± 0.15	-5.30 ± 0.18	1.93 ± 0.14	2.17 ± 0.10	1.68 ± 0.13	1.41 ± 0.19
44–45	-5.42 ± 0.19	-5.50 ± 0.24	-6.08 ± 0.40	-5.15 ± 0.14	1.82 ± 0.20	1.72 ± 0.25	1.58 ± 0.40	2.26 ± 0.16
45–46	–	–	–	-6.20 ± 0.43	–	–	–	1.85 ± 0.43

The columns are: (1): X-ray luminosity interval; (2): logarithm of XLF in units of $\times 10^{-6} \text{ Mpc}^{-3}$ for disks, early-type, peculiar and point sources; (3) luminosity density in units of $\times 10^{37} \text{ erg s}^{-1} \text{ Mpc}^{-3}$ for the morphological classes above.

Table 3. Fractional contribution of different morphological types to the total AGN XLF and luminosity density

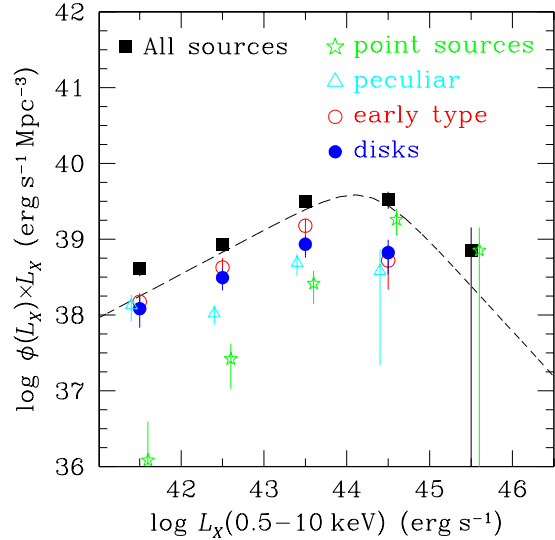
$\log L_X$ (erg s^{-1})	fraction of $\phi_{\text{total}}(L_X)$				fraction of $L_X \phi_{\text{total}}(L_X)$			
	disk	early	peculiar	point	disk	early	peculiar	point
41–42	0.28 ± 0.12	0.30 ± 0.10	0.41 ± 0.22	0.001 ± 0.001	0.29 ± 0.13	0.36 ± 0.11	0.33 ± 0.12	0.002 ± 0.006
42–43	0.34 ± 0.08	0.46 ± 0.11	0.16 ± 0.05	0.02 ± 0.01	0.35 ± 0.11	0.49 ± 0.15	0.12 ± 0.03	0.03 ± 0.01
43–44	0.29 ± 0.10	0.47 ± 0.10	0.17 ± 0.06	0.04 ± 0.02	0.27 ± 0.09	0.48 ± 0.11	0.15 ± 0.04	0.08 ± 0.03
44–45	0.25 ± 0.11	0.21 ± 0.12	0.05 ± 0.05	0.47 ± 0.15	0.19 ± 0.09	0.15 ± 0.09	0.11 ± 0.10	0.53 ± 0.20
45–46	–	–	–	1.00 ± 1.00	–	–	–	1.00 ± 1.00
41–45	0.30 ± 0.09	0.35 ± 0.07	0.34 ± 0.15	0.010 ± 0.005	0.23 ± 0.05	0.31 ± 0.06	0.13 ± 0.05	0.33 ± 0.12

The columns are: (1): X-ray luminosity interval; (2): fractional contribution to the XLF for disks, early-type, peculiar and point sources; (3) fractional contribution to the luminosity density for the morphological classes above.

**Figure 6.** The 0.5–10 keV X-ray luminosity function for different host galaxy types normalised to the total XLF. The vertical axis measures the contribution of different galaxy types to the XLF. The symbols are the same as in Figure 5.

the AGN lightcurve declines with time, t , as $L \propto t^{-\beta}$ with $\beta = 0.6$, while in the revised curve shown in the figure $\beta = 1.5$. The updated model reproduces the overall shape of the observed AGN XLF of disk galaxies but lies below the observations. Also, both models of the stochastic AGN accretion mode shown in Figure 5 underpredict the number density of AGN in disk galaxies at bright luminosities, $> 10^{44} \text{ erg s}^{-1}$. This suggests that bar instabilities and minor interactions are more efficient in producing powerful AGN than the Hopkins & Hernquist (2006) model predicts.

Alternatively, one might argue that a fraction of the X-ray

**Figure 7.** The 0.5–10 keV X-ray luminosity density for different host galaxy types. The symbols and curves are the same as in Figure 5.

AGN in disk hosts represent major merger events. Recent simulations indeed show that under certain conditions disks can survive or reform after a major merger. Some authors show that the formation of a remnant with a large disk requires very high cold gas fractions (> 50 per cent in mass) in the progenitors (e.g. Springel & Hernquist 2005; Hopkins et al. 2008), which may be typical of high redshift ($z \gtrsim 2$) objects. Others show that cold gas flowing onto the remnant from Mpc scales can quickly reform a disk even if the progenitors have moderate amounts of cold gas reservoirs (Governato et al. 2008). At the same time however, it is also argued that the conditions that lead to the formation of a disk merger remnant are not associated with substantial SMBH

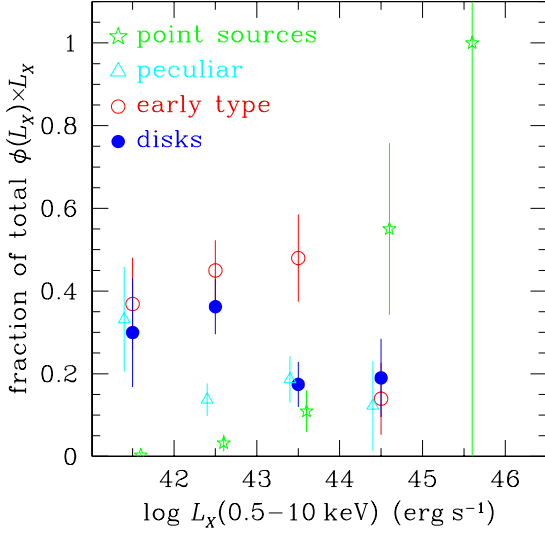


Figure 8. The fractional contribution of different AGN host galaxy morphological types to the 0.5-10 keV X-ray luminosity density. The symbols are the same as in Figure 5.

growth (e.g. Hopkins & Hernquist 2008a). The dark matter halo of the simulation of Governato et al. (2008) for example, has a mass of $< 10^{12} M_\odot$, while X-ray AGN have been shown to reside in halos more massive than that (e.g. Silverman et al. 2008a; Gilli et al. 2008; Coil et al. 2009; Hickox et al. 2009), where cold gas flows are expected to be suppressed because of shock heating (e.g. Dekel & Birnboim 2006; Croton et al. 2006; Cattaneo et al. 2007). Additionally, in the simulation of Governato et al. (2008) the black hole mass of the merger remnant at $z = 0$ is expected to be $4 \times 10^7 M_\odot$, assuming the relation between SMBH mass and bulge mass of Häring & Rix (2004), while X-ray AGN at $z \approx 1$ are believed to be associated with black holes more massive than that (Babić et al. 2007; Bundy et al. 2008; Coil et al. 2009; Hickox et al. 2009, e.g.). AGN in disk hosts therefore pose a strong constraint on the fraction of SMBHs that are fueled by mechanisms other than major mergers. Cosmological simulations of galaxy formation and SMBH growth will need to reproduce the observed luminosity distribution of AGN in spirals by invoking either minor interactions, bar instabilities or the reformation of disks in major mergers.

If AGN in disk galaxies are systems where the accretion on the SMBH is triggered by secular evolution or minor tidal disruptions then their estimated fraction to the XLF represents only a lower limit to the contribution of these SMBH fueling processes to the accretion density at $z \approx 1$. Although bulge-dominated galaxies are likely to be the products of a major merger, the observed nuclear activity in these systems may not be associated with this past event. The AGN in some early-type galaxies for example, may be fueled by cold gas accretion via minor tidal interactions. The simulations of Khalatyan et al. (2008) demonstrate that this process can activate the SMBH of early-type galaxies, thereby producing AGN with luminosities similar to those probed here. Ciotti & Ostriker (2007) also showed that secular evolution in isolated elliptical galaxies could drive recycled gas to the central regions, thereby producing recursive nuclear starbursts and accretion onto the SMBH. Similarly, not all QSOs ($L_X > 10^{44} \text{ erg s}^{-1}$; point sources in our sam-

ple) are likely to be the products of major mergers. Studies of such sources in the nearby Universe have revealed that some of them are hosted by non-interacting spirals (e.g. Canalizo & Stockton 2001), while more recent observations suggest that about 30 per cent of QSOs at low redshift are in disk galaxies (e.g. Guyon et al. 2006). Therefore, the fraction of AGN associated with early-type galaxies, peculiars and point sources is an upper limit to the contribution of major mergers to the accretion density.

Recent studies on star-forming galaxies also downplay the contribution of major mergers to the evolution of these systems since $z \approx 1$ (Melbourne et al. 2005; Bell et al. 2005; Elbaz et al. 2007; Buat et al. 2008). It is found that about half of the starburst population at these redshifts is associated with spirals, underlining the importance of minor interactions and bar instabilities in galaxy evolution. If the build-up of the stellar mass of galaxies and the growth of SMBH at their centres are related (e.g. Gebhardt et al. 2000; Ferrarese & Merritt 2000) then the findings above support the idea that a potentially large fraction of the AGN at $z \approx 1$ are triggered by processes other than major mergers.

7 ACKNOWLEDGMENTS

The authors wish to thank the anonymous referee for providing constructive comments and suggestions that significantly improved this paper and Philip F. Hopkins for making available unpublished results on the XLF for the stochastic fuelling of SMBH. The authors acknowledge use of data from the Team Keck Treasury Redshift Survey (TKRS; <http://www2.keck.hawaii.edu/science/tksurvey/>) and the ESO/GOODS project which is based on observations carried out at the Very Large Telescope at the ESO Paranal Observatory under Program IDs: 170.A-0788, 074.A-0709, 275.A-5060 and 171.A-3045. Support for this work was provided by NASA through the Spitzer Space Telescope Fellowship Program. The source catalogues used in the paper are available at www.astro.noa.gr/~age.

Based on observations obtained with MegaPrime/MegaCam, a joint project of CFHT and CEA/DAPNIA, at the Canada-France-Hawaii Telescope (CFHT) which is operated by the National Research Council (NRC) of Canada, the Institut National des Sciences de l'Univers of the Centre National de la Recherche Scientifique (CNRS) of France, and the University of Hawaii. This work is based in part on data products produced at TERAPIX and the Canadian Astronomy Data Centre as part of the Canada-France-Hawaii Telescope Legacy Survey, a collaborative project of NRC and CNRS.

REFERENCES

- Abraham R. G., van den Bergh S., Glazebrook K., Ellis R. S., Santiago B. X., Surma P., Griffiths R. E., 1996, *ApJS*, 107, 1
- Aird J., Nandra K., Georgakakis A., Laird E. S., Steidel C. C., Sharon C., 2008, *MNRAS*, 387, 883
- Akylas A., Georgantopoulos I., Georgakakis A., Kitsionas S., Hatziminaoglou E., 2006, *A&A*, 459, 693
- Babić A., Miller L., Jarvis M. J., Turner T. J., Alexander D. M., Croom S. M., 2007, *A&A*, 474, 755
- Barger A. J., Cowie L. L., Capak P., Alexander D. M., Bauer F. E., Fernandez E., Brandt W. N., Garmire G. P., Hornschemeier A. E., 2003, *AJ*, 126, 632

- Barger A. J., Cowie L. L., Mushotzky R. F., Yang Y., Wang W.-H., Steffen A. T., Capak P., 2005, *AJ*, 129, 578
- Barnes J. E., Hernquist L., 1996, *ApJ*, 471, 115
- Barnes J. E., Hernquist L. E., 1991, *ApJ*, 370, L65
- Bell E. F., et al., 2005, *ApJ*, 625, 23
- Bennert N., Canalizo G., Jungwiert B., Stockton A., Schweizer F., Peng C. Y., Lacy M., 2008, *ApJ*, 677, 846
- Borne K. D., Bushouse H., Lucas R. A., Colina L., 2000, *ApJ*, 529, L77
- Brinchmann J., et al., 1998, *ApJ*, 499, 112
- Brusa M., et al., 2008, *ArXiv0809.2513*
- Buat V., Boissier S., Burgarella D., Takeuchi T. T., Le Floch E., Marcellac D., Huang J., Nagashima M., Enoki M., 2008, *A&A*, 483, 107
- Bundy K., et al., 2008, *ApJ*, 681, 931
- Canalizo G., Bennert N., Jungwiert B., Stockton A., Schweizer F., Lacy M., Peng C., 2007, *ApJ*, 669, 801
- Canalizo G., Stockton A., 2001, *ApJ*, 555, 719
- Cattaneo A., Blaizot J., Weinberg D. H., Kereš D., Colombi S., Davé R., Devriendt J., Guiderdoni B., Katz N., 2007, *MNRAS*, 377, 63
- Cattaneo A., Teyssier R., 2007, *MNRAS*, 376, 1547
- Ciliegi P., Zamorani G., Hasinger G., Lehmann I., Szokoly G., Wilson G., 2003, *A&A*, 398, 901
- Ciotti L., Ostriker J. P., 2007, *ApJ*, 665, 1038
- Coil A. L., et al., 2009, *ArXiv0902.036*
- Coleman G. D., Wu C.-C., Weedman D. W., 1980, *ApJS*, 43, 393
- Cowie L. L., Barger A. J., Bautz M. W., Brandt W. N., Garmire G. P., 2003, *ApJ*, 584, L57
- Croton D. J., et al., 2006, *MNRAS*, 365, 11
- Davis M., et al., 2003, in *Society of Photo-Optical Instrumentation Engineers (SPIE) Conference Series*, Guhathakurta P., ed., Vol. 4834, pp. 161–172
- , 2007, *ApJ*, 660, L1
- Dekel A., Birnboim Y., 2006, *MNRAS*, 368, 2
- Di Matteo T., Springel V., Hernquist L., 2005, *Nature*, 433, 604
- Dickinson M., et al., 2004, *ApJ*, 600, L99
- Elbaz D., et al., 2007, *A&A*, 468, 33
- Faber S. M., et al., 2003, in *Society of Photo-Optical Instrumentation Engineers (SPIE) Conference*, Vol. 4841, *Instrument Design and Performance for Optical/Infrared Ground-based Telescopes*, Iye M., Moorwood A. F. M., eds., pp. 1657–1669
- Farrah D., Rowan-Robinson M., Oliver S., Serjeant S., Borne K., Lawrence A., Lucas R. A., Bushouse H., Colina L., 2001, *MNRAS*, 326, 1333
- Ferrarese L., Merritt D., 2000, *ApJ*, 539, L9
- Franceschini A., Braito V., Persic M., Della Ceca R., Bassani L., Cappi M., Malaguti P., Palumbo G. G. C., Risaliti G., Salvati M., Severgnini P., 2003, *MNRAS*, 343, 1181
- Gabor J. M., et al., 2008, *ArXiv0809.0309*
- Gebhardt K., Bender R., Bower G., Dressler A., Faber S. M., Filippenko A. V., Green R., Grillmair C., Ho L. C., Kormendy J., Lauer T. R., Magorrian J., Pinkney J., Richstone D., Tremaine S., 2000, *ApJ*, 539, L13
- Georgakakis A., Nandra K., Laird E. S., Aird J., Trichas M., 2008a, *MNRAS*, 388, 1205
- Georgakakis A., Rowan-Robinson M., Babbedge T. S. R., Georgantopoulos I., 2007, *MNRAS*, 377, 203
- Georgakakis A., et al., 2006, *MNRAS*, 371, 221
- , 2008b, *MNRAS*, 385, 2049
- Giavalisco M., et al., 2004, *ApJ*, 600, L93
- Gilli R., et al., 2008, *ArXiv:0810.4769*
- Governato F., Brook C. B., Brooks A. M., Mayer L., Willman B., Jonsson P., Stilp A. M., Pope L., Christensen C., Wadsley J., Quinn T., 2008, *arXiv:0812.0379*
- Guyon O., Sanders D. B., Stockton A., 2006, *ApJS*, 166, 89
- Häring N., Rix H.-W., 2004, *ApJ*, 604, L89
- Hasinger G., 2008, *A&A*, 490, 905
- Hasinger G., Miyaji T., Schmidt M., 2005, *A&A*, 441, 417
- Hennawi J. F., et al., 2006, *AJ*, 131, 1
- Hernquist L., 1989, *Nature*, 340, 687
- Hickox R. C., Markevitch M., 2006, *ApJ*, 645, 95
- Hickox R. C., et al., 2009, *ArXiv0901.4121*
- Ho L. C., Filippenko A. V., Sargent W. L. W., 1997, *ApJS*, 112, 315
- Hopkins A. M., Connolly A. J., Szalay A. S., 2000, *AJ*, 120, 2843
- Hopkins P. F., Cox T. J., Younger J. D., Hernquist L., 2008, *arXiv:0806.1739*
- Hopkins P. F., Hernquist L., 2006, *ApJS*, 166, 1
- , 2008a, *arXiv:0812.2915*
- , 2008b, *ArXiv:0809.3789*
- Hopkins P. F., Hernquist L., Cox T. J., Di Matteo T., Robertson B., Springel V., 2006, *ApJS*, 163, 1
- Ilbert O., et al., 2006, *A&A*, 457, 841
- Khalatyan A., Cattaneo A., Schramm M., Gottlöber S., Steinmetz M., Wisotzki L., 2008, *MNRAS*, 387, 13
- Kuhlbrodt B., Wisotzki L., Jahnke K., 2004, *MNRAS*, 349, 1027
- Laird E. S., et al., 2008, *ArXiv0809.1349*
- Le Fèvre O., et al., 2004, *A&A*, 428, 1043
- Li C., Kauffmann G., Heckman T. M., White S. D. M., Jing Y. P., 2008, *MNRAS*, 385, 1915
- Lilly S. J., Tresse L., Hammer F., Crampton D., Le Fevre O., 1995, *ApJ*, 455, 108
- Lotz J. M., Jonsson P., Cox T. J., Primack J. R., 2008a, *ArXiv0805.1246*
- Lotz J. M., Primack J., Madau P., 2004, *AJ*, 128, 163
- Lotz J. M., et al., 2008b, *ApJ*, 672, 177
- Marconi A., Risaliti G., Gilli R., Hunt L. K., Maiolino R., Salvati M., 2004, *MNRAS*, 351, 169
- Melbourne J., Koo D. C., Le Floch E., 2005, *ApJ*, 632, L65
- Mignoli M., et al., 2005, *A&A*, 437, 883
- Morrison R., McCammon D., 1983, *ApJ*, 270, 119
- Myers A. D., Brunner R. J., Richards G. T., Nichol R. C., Schneider D. P., Bahcall N. A., 2007, *ApJ*, 658, 99
- Nandra K., Pounds K. A., 1994, *MNRAS*, 268, 405
- Peng C. Y., Ho L. C., Impey C. D., Rix H.-W., 2002, *AJ*, 124, 266
- Pierce C. M., Lotz J. M., Laird E. S., Lin L., Nandra K., Primack J. R., Faber S. M., Barmby P., Park S. Q., Willner S. P., Gwyn S., Koo D. C., Coil A. L., Cooper M. C., Georgakakis A., Koekemoer A. M., Noeske K. G., Weiner B. J., Willmer C. N. A., 2007, *ApJ*, 660, L19
- Popesso P., et al., 2008, *ArXiv0802.2930*
- Robertson B., Bullock J. S., Cox T. J., Di Matteo T., Hernquist L., Springel V., Yoshida N., 2006, *ApJ*, 645, 986
- Rowan-Robinson M., et al., 2005, *AJ*, 129, 1183
- , 2008, *MNRAS*, 386, 697
- Sanders D. B., Mirabel I. F., 1996, *ARA&A*, 34, 749
- Schmidt M., 1968, *ApJ*, 151, 393
- Serber W., Bahcall N., Ménard B., Richards G., 2006, *ApJ*, 643, 68
- Silverman J. D., et al., 2008a, *ArXiv:0812.3402*
- , 2008b, *ApJ*, 679, 118
- Simard L., Willmer C. N. A., Vogt N. P., Sarajedini V. L., Phillips

- A. C., Weiner B. J., Koo D. C., Im M., Illingworth G. D., Faber S. M., 2002, *ApJS*, 142, 1
- Simmons B. D., Urry C. M., 2008, *ApJ*, 683, 644
- Somerville R. S., Hopkins P. F., Cox T. J., Robertson B. E., Hernquist L., 2008, *ArXiv0808.1227*
- Springel V., Hernquist L., 2005, *ApJ*, 622, L9
- Springel V., et al., 2005, *Nature*, 435, 629
- Stanway E. R., Bunker A. J., McMahon R. G., Ellis R. S., Treu T., McCarthy P. J., 2004a, *ApJ*, 607, 704
- Stanway E. R., et al., 2004b, *ApJ*, 604, L13
- Surace J. A., Sanders D. B., Vacca W. D., Veilleux S., Mazzarella J. M., 1998, *ApJ*, 492, 116
- Sutherland W., Saunders W., 1992, *MNRAS*, 259, 413
- Szokoly G. P., et al., 2004, *ApJS*, 155, 271
- Ueda Y., Akiyama M., Ohta K., Miyaji T., 2003, *ApJ*, 598, 886
- Vanden Berk D. E., et al., 2001, *AJ*, 122, 549
- Vanzella E., et al., 2005, *A&A*, 434, 53
- , 2008, *A&A*, 478, 83
- Vogt N. P., et al., 2005, *ApJS*, 159, 41
- Weiner B. J., et al., 2005, *ApJ*, 620, 595
- Wirth G. D., et al., 2004, *AJ*, 127, 3121
- Wolf C., et al., 2004, *A&A*, 421, 913
- York D. G., et al., 2000, *AJ*, 120, 1579
- Younger J. D., Hopkins P. F., Cox T. J., Hernquist L., 2008, *ApJ*, 686, 815